Available online at www.sciencedirect.com
ScienceDirect
Applied Catalysis B: Environmental 82 (2008) 139–150
APPLIED CATALYSIS B: ENVIRONMENTAL
www.elsevier.com/locate/apcatb

Highly active deep HDS catalysts prepared using Mo and W heteropolyacids supported on SBA-15

Lilia Lizama, Tatiana Klimova *

Facultad de Química, Departamento de Ingeniería Química, Universidad Nacional Autónoma de México (UNAM), México D.F. 04510, Mexico

Received 12 October 2007; received in revised form 22 January 2008; accepted 23 January 2008
Available online 2 February 2008

Abstract

A series of Mo (W) catalysts promoted by Ni and supported on pure siliceous SBA-15 was prepared using Keggin-type heteropolyacids ($H_3PMo_{12}O_{40}$ or $H_3PW_{12}O_{40}$) as active phase precursors. These catalysts were compared with corresponding NiMo(W)/SBA-15 catalysts prepared from the traditional precursors (ammonium heptamolybdate, ammonium metatungstate). Prepared catalysts were characterized by N_2 physisorption, small- and wide-angle XRD, UV–vis DRS, FT-IR, TPR, ^{31}P MAS NMR, HRTEM and evaluated in hydrodesulfurization of 4,6-dimethyldibenzothiophene (4,6-DMDBT). It was found that both Mo and W catalysts prepared from heteropolyacids showed better performance in deep HDS of 4,6-DMDBT than the counterparts prepared from traditionally used Mo (W) ammonium salts. The possible reasons of this phenomenon are discussed.

Keywords: Ultra-deep hydrodesulfurization; 4,6-DMDBT; SBA-15; Keggin-type heteropolyacid

1. Introduction

Nowadays, the growing demand for cleaner transport fuels drives the need to improve hydrotreating processes. In particular, sulfur removal from fossil fuels is strongly desirable not only due to the well-known environmental implications of SO_X pollution but also because of the adverse effects that sulfur presence has on the durability of refinery equipment and catalytic converters. Some of the key factors for sulfur elimination as well as the new approaches and emerging technologies that allow obtaining ultra-low sulfur fuels are discussed in Refs. [1,2]. In the case of diesel fuels, the sulfur level is expected to be lowered to 10 ppm in a large part of the world by the end of this decade. In order to fulfill these new stringent legislative requirements, ultra-deep hydrodesulfurization (HDS) should be performed instead of a conventional HDS, in which sulfur content is reduced up to 300–500 ppm over Ni(Co)Mo/alumina catalysts. As a result of the extensive research that has been carried out in academic institutions and catalyst and petroleum companies, nowadays a number of catalysts with improved activity and selectivity are available in the market. Some of the new commercial catalysts developed for ultra-deep HDS are described in Ref. [2]. Even though the production of ultra-low sulfur diesel can be achieved, the process needs to be carried out under more severe conditions, i.e. higher hydrogen pressure, higher reaction temperature and/or lower liquid hourly space velocity (LHSV), which yield some negative consequences such as coke formation and reduced hydrotreating efficiency. Therefore, the development of more active catalysts, able to desulfurize refractory sulfur-containing molecules (such as dibenzothiophenes with alkyl groups in positions 4 and 6 of the molecule), operating in a cost-effective manner is still an actual task.

Nowadays it is well known that there are different options that allow modifying the behavior of HDS catalysts in a desirable way. Among them, using new catalytic supports [3] or changing the nature of the active phase [4–6]. Recent results concerning the developments of new supports and their effects on HDS catalysts have been summarized in Ref. [7]. Another common industrial practice is the introduction of additives like phosphorus to the catalytic formulation. In some cases, an improvement in the HDS activity of alumina-supported Mo-based catalysts was observed after phosphorus incorporation [8]. Kwak et al. [9] observed that phosphorus modifies catalytic

* Corresponding author. Tel.: +52 55 56225371; fax: +52 55 56225371.
E-mail address: klimova@servidor.unam.mx (T. Klimova).

0926-3373/$ – see front matter © 2008 Elsevier B.V. All rights reserved.
doi:10.1016/j.apcatb.2008.01.018

behavior of $CoMo/Al_2O_3$ catalysts in two ways: increase of active sites by enhanced metal dispersion and increase of Brönsted acidity. These effects yield a different distribution of products depending on the reactants. In thiophene HDS, phosphorus increases only the overall conversion. In dibenzothiophene (DBT) HDS, phosphorus increases the conversion along with the promotion of the hydrogenation (HYD) pathway of the reaction. In the case of 4,6-dimethyldibenzothiophene (4,6-DMDBT) HDS, the conversion also increases but the direct desulfurization (DDS) pathway results to be promoted due to phosphorus addition, the opposite trend from the one observed in DBT HDS. This is attributed to enhanced acidity of the catalyst, which allows migration of the methyl groups in 4,6-DMDBT.

Another approach to catalyst modification is the use of different catalytic precursors. Mo (W) oxides or salts are commonly used as precursors in the preparation of Mo (W)-based HDS catalysts. Keggin-type heteropolyacids (HPAs) are well-known industrial catalysts generally applied in two major areas: acid catalysis and catalytic oxidation [10,11]. However, up to now, there have been very few reports on the application of heteropolyacids in the preparation of HDS catalysts [12–19]. Different carriers have been used to support HPAs. It was found that when HPAs are deposited on alumina their characteristic heteropolyanion structure is destroyed, and the catalytic behavior of these catalysts is similar to that of the conventional Mo (W) ones [14]. The stability of Keggin molecules supported on alumina can be improved by using unreduced and reduced Co or Ni salts as catalytic precursors. Even though these units maintain their characteristic structure in supported state and give better results than the destroyed acids, the main drawback in the use of this kind of starting materials is that the Ni (Co) content is limited and the highest Ni (Co)/Mo ratio obtained with the reduced salts is less than 0.3, which remains below the optimum one (Co/Mo = 0.5) [13,19].

Mesoporous molecular sieves such as SBA-15 [20,21], highly stable and with better textural properties compared to γ-alumina seem to be suitable for depositing HPA precursors. Derouane and co-workers [16] showed that silica-supported $H_3PW_{12}O_{40}$ (HPW) is an efficient precursor that yields active catalysts for HDS of dibenzothiophene, comparable to commercial $CoMo/Al_2O_3$ catalyst under industrially relevant conditions. Damyanova and co-workers [18] demonstrated that HPMo and HPW supported on mesoporous silica (HMS) materials modified with Al, Zr and Ti are also good precursors for the active phase for HDS of DBT. In our group, a series of Mo (W) catalysts promoted by Ni (Co), supported on SBA-15 was prepared using Keggin-type HPAs and tested in 4,6-dimethyldibenzothiophene HDS [22]. It was found that unpromoted and Co-promoted catalysts had low catalytic activity due to the high temperature required for their activation. However, both Mo and W, Ni-promoted catalysts could be activated at lower temperatures (about 400 °C) and showed substantially higher activities than those of the alumina-supported analogues in HDS of 4,6-dimethyldibenzothiophene, one of the most refractory sulfur compounds. To our knowledge, no other work on ultra-deep HDS with catalysts obtained from HPA precursors has been published. The aim of the present work is to demonstrate that SBA-15-supported HPAs are better oxide precursors than conventional W and Mo salts for the preparation of highly active catalysts for HDS of 4,6-dimethyldibenzothiophene.

2. Experimental

2.1. Support and catalyst preparation

The pure siliceous hexagonal *p6mm* SBA-15 was prepared according to literature [20] using the triblock copolymer Pluronic P123 (M_{av} = 5800, $EO_{20}PO_{70}EO_{20}$, Aldrich) as the structure-directing agent and tetraethyl orthosilicate (TEOS, Aldrich) as the silica source. Four grams of Pluronic P123 were dissolved in 30 g of water and 120 g of 2 M HCl solution at 35 °C. Then 8.50 g of TEOS were added into the solution. The mixture was stirred at 35 °C for 20 h and then aged at 80 °C for 48 h without stirring. The solid product was recovered by filtration, washed with deionized water and air-dried at room temperature. Calcination was carried out in static air at 550 °C for 6 h. Mo (W) were incorporated to the SBA-15 support by incipient wetness impregnation of methanol solutions of Keggin-type HPAs, $H_3PMo_{12}O_{40}{\cdot}xH_2O$ (Aldrich) and $H_3PW_{12}O_{40}{\cdot}xH_2O$ (Sigma), respectively. The choice of methanol as the solvent for depositing Keggin HPAs on SBA-15 was made in order to avoid the presence of different structures on the silica surface as found when water solutions are used at low HPA loadings (<30 wt.%) [23]. The promoter was incorporated in a second step by impregnation of methanol solution of nickel nitrate, $Ni(NO_3)_2{\cdot}6H_2O$ (Baker). After each impregnation, the samples were calcined for 2 h at 350 °C in air. The samples were designated as HPM/SBA-15 for unpromoted catalysts and NiPM/SBA-15 for promoted catalysts, where M = Mo or W. Reference catalysts were prepared by successive impregnations of aqueous solutions of conventional precursors: ammonium heptamolybdate (AHM), $(NH_4)_6Mo_7O_{24}{\cdot}4H_2O$ (Merck) or ammonium metatungstate (AMT), $(NH_4)_6H_2W_{12}O_{40}$ (Fluka) and nickel nitrate, $Ni(NO_3)_2{\cdot}6H_2O$ (Baker). These were designated as M/SBA-15 and NiM/SBA-15 (M = Mo, W). After each impregnation, the catalysts were dried and calcined as described above. The nominal composition of the catalysts was 12 wt.% of MoO_3 and 3 wt.% of NiO for Mo series, and 20 wt.% of WO_3 and 5 wt.% of NiO for W catalysts. By this means, the molar charge of the active phase (~0.6 molecules of MO_3/nm^2) and the molar ratio active phase: promoter equal to 2:1 were preserved allowing comparison between catalysts of Mo and W series.

2.2. Characterization

The support and catalysts were characterized by N_2 physisorption, small- and wide-angle XRD, UV–vis DRS, FT-IR, TPR, ^{31}P MAS NMR and HRTEM. N_2 adsorption/desorption isotherms were measured with a Micromeritics ASAP 2000 automatic analyzer at liquid N_2 temperature. Prior to the experiments, the samples were degassed ($p < 10^{-1}$ Pa)

at 270 °C for 6 h. Specific surface areas (S_{BET}) were calculated by the BET method and the pore volume (V_p) was determined by nitrogen adsorption at a relative pressure of 0.98. The mesopore diameter (D_{ads}) corresponds to the maximum of the pore size distributions obtained from the adsorption isotherms by the BJH method. The micropore area (S_μ) was estimated using the correlation of *t*-Harkins & Jura (*t*-plot method). XRD patterns were recorded in the $3^\circ \leq 2\Theta \leq 90^\circ$ range in a Siemens D5000 diffractometer, using Cu Kα radiation (λ = 1.5406 Å) and a goniometer speed of $1^\circ(2\Theta)\ min^{-1}$. Small-angle XRD ($2\Theta = 0.5–10^\circ$) was performed on the Bruker D8 Advance diffractometer using small divergence and scattering slits of 0.05°. The a_0 unit-cell parameter was estimated from the position of the (1 0 0) diffraction line ($a_0 = d_{100} \times 2/\sqrt{3}$). Pore wall thickness, δ, was assessed by subtracting D_{ads} from the a_0 unit-cell parameter which corresponds to the distance between centers of adjacent mesopores. UV–vis electronic spectra of the samples were recorded in the wavelength range 200–800 nm using a Varian Cary 100 spectrophotometer equipped with a diffuse reflectance attachment. Polytetrafluoroethylene was used as reference. IR spectra of the support and catalysts were recorded after transfer in air, in a transmittance mode with a PerkinElmer FT-IR 1605 Nicolet Magna 750 Fourier transform spectrometer. TPR experiments were carried out in a Micromeritics AutoChem II 2920 automatic analyzer equipped with a TC detector. In the TPR experiments, the samples were pretreated in situ at 350 °C for 2 h under air flow and cooled in an Ar stream. The reduction step was performed under a stream of an Ar/H_2 mixture (70/30 mol/mol and 25 ml/min), with a heating rate of 10 °C/min, up to 1000 °C. Solid-state ^{31}P MAS NMR spectra were obtained with an ASX300 Bruker NMR spectrometer using H_3PO_4 as an external ^{31}P reference, at a source frequency of 121.5 MHz and a spinning rate of 5 kHz with radio frequency pulses of 4.0 μs. The spectra were recorded after transfer in air at 25 °C, in order to resemble the conditions in which catalysts are handled before the activation step. High-resolution transmission electron microscopy (HRTEM) studies were performed using a Jeol 2010 microscope (resolving power 1.9 Å). The solids were ultrasonically dispersed in heptane and the suspension was collected on carbon-coated grids. Layer stacking distributions and slab length of MoS_2 crystallites in each sample were established from the measurement of at least 300 crystallites detected on several HRTEM pictures taken from different regions of each sample.

2.3. Catalytic activity

Prior to the catalytic activity tests, the catalysts were sulfided ex situ in a tubular reactor at 400 °C for 4 h in a stream of 15 vol.% of H_2S in H_2 under atmospheric pressure. The 4,6-DMDBT HDS activity tests were performed in a batch reactor (Parr) at 300 °C and 7.3 MPa total pressure for 8 h. The reactor was filled in an inert atmosphere with 40 ml of a solution of 4,6-DMDBT in hexadecane (with a total sulfur content of 500 ppm) and 0.15 g of sulfided catalysts. The course of the reaction was followed by taking aliquots each hour and analyzing them in an HP-6890 chromatograph equipped with a FID detector and a non-polar methyl siloxane capillary column HP-1 (50 m × 0.32 mm i.d. and 0.52 μm film thickness). The amount of gaseous products was negligibly small under the present conditions. To corroborate liquid product identification, the product mixture was analyzed in a Hewlett Packard GC–MS equipment. The identified reaction products were 4,6-dimethyl-1,2,3,4-tetrahydrodibenzothiophene (THDMDBT), 4,6-dimethyl-1,2,3,4,4a,9b-hexahydrodibenzothiophene (HHDMDBT), 1-methyl-3-(3′-methylcyclohexyl)benzene (MCHT, two isomers), 3,3′-dimethyl-1,1′-bicyclohexyl (DMBCH, two isomers) and 3,3′-dimethyl-1,1′-biphenyl (DMBP). The quantitative analysis of the reactant and products was performed using corresponding calibration curves and hexadecane as an internal standard in all cases.

3. Results

3.1. Textural and structural characteristics

The small-angle XRD patterns of the SBA-15 support and catalysts are shown in Fig. 1. All samples exhibit three clearly defined peaks characteristic of hexagonally ordered *p6mm* structure; a strong (1 0 0) reflection at 0.96° (2θ) and two small shoulders between 1.5° and 2° (2θ) which yield an a_0 value of 106 Å (Table 1).

The nitrogen adsorption–desorption isotherms for the support and Ni-promoted Mo and W catalysts are shown in Fig. 2. All isotherms correspond to type IV and exhibit an H1 hysteresis loop characteristic of SBA-15 mesoporous material. The sharpness of the adsorption branches is indicative of a narrow mesopore size distribution, with a pore size of 81 Å for the support and 74–75 Å for promoted catalysts (Table 1). The pore wall thickness was calculated according to Ref. [24], showing values of 25 Å for the SBA-15 and about 32 Å for the catalysts. This notable increase in the pore wall thickness suggests that the metal oxide species are located inside the mesopores.

Results from textural characterization of the catalysts (Table 1) indicate that the incorporation of Mo (W) species and Ni promoter on the SBA-15 surface produces a decrease in specific surface area (S_{BET}), micropore area (S_μ) and pore volume (V_p), which becomes more significant for the samples

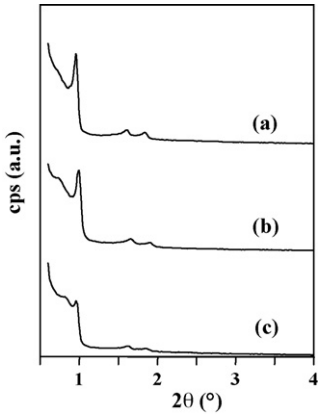

Fig. 1. Small-angle XRD patterns of SBA-15 (a), NiPMo/SBA-15 (b) and NiPW/SBA-15 (c).

Table 1
Textural and structural characteristics of SBA-15 support and promoted catalysts

Sample	S_{BET} [a] (m^2/g)	S_μ [b] (m^2/g)	V_p [c] (cm^3/g)	D_{ads} [d] (Å)	a_0 [e] (Å)	δ [f] (Å)
SBA-15	837	131	1.09	81	106	25
NiPMo/SBA-15	684	106	0.94	74	106	32
NiMo/SBA-15	554	78	0.80	74	106	32
NiPW/SBA-15	556	111	0.73	74	106	32
NiW/SBA-15	513	87	0.64	75	106	31

[a] S_{BET}, specific surface area calculated by the BET method.
[b] S_μ, micropore area estimated using the correlation of *t*-Harkins & Jura (*t*-plot method).
[c] V_p, pore volume determined by nitrogen adsorption at a relative pressure of 0.98.
[d] D_{ads}, mesopore diameter corresponding to the maximum of the pore size distribution obtained from the adsorption isotherm by the BJH method.
[e] a_0, unit-cell parameter determined from the position of the (1 0 0) diffraction line as $a_0 = d_{100} \times 2/\sqrt{3}$.
[f] δ, pore wall thickness calculated as $\delta = a_0 - D_{ads}$.

prepared using the conventional precursors (ammonium heptamolybdate or ammonium metatungstate). In addition, a comparison between the catalysts of Mo and W series (Table 1; Fig. 2) shows that in all the cases independently of the metal precursor used, W-containing samples have lower values of surface area and pore volume than the corresponding Mo-containing ones. However, this can be due to the fact that the W-based catalysts prepared in the present study have higher WO_3 loading (20 wt.%) compared to their Mo-based analogues (12 wt.% of MoO_3) in order to preserve the same molar charge of the active phase (~0.6 molecules of metal oxide/nm^2). Therefore, the specific values of S_{BET} and V_p of the parent SBA-15 support (calculated per gram of the sample) seem to suffer larger modification after the incorporation of W species compared to corresponding Mo ones.

3.2. Integrity of the Keggin unit in dried and calcined catalysts

The thermal decomposition of Mo and W bulk HPAs follows a known scheme reported elsewhere [11,25]. The loss of physisorbed water occurs at temperatures around 100–120 °C, while further increase in temperature causes the loss of hydration water molecules. Up to this point the Keggin units might be hydrated and reconstructed by exposure to water vapor or even with the environmental moisture. The loss of water molecules corresponding to the loss of acidic protons from $H_3PW_{12}O_{40}$ occurs at 450–470 °C and is practically irreversible [11]. Similar behavior is observed for $H_3PMo_{12}O_{40}$ at about 440 °C. As it is of our interest to study the effect of keeping the integrity of the Keggin unit until the activation step and the catalysts are regularly handled under air atmosphere, the IR and ^{31}P MAS NMR characterizations were performed under similar conditions.

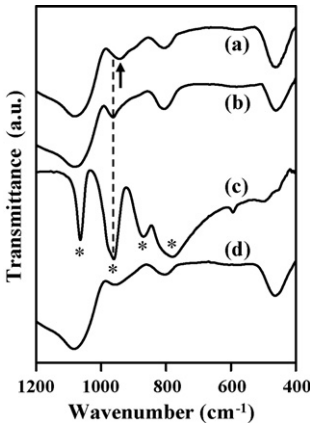

Fig. 3. IR spectra of calcined NiPMo/SBA-15 (a) and HPMo/SBA-15 (b) catalysts; bulk $H_3PMo_{12}O_{40}$ (c) and SBA-15 (d).

The IR spectra of the support, bulk $H_3PW_{12}O_{40}$ and calcined HPMo/SBA-15 and NiPMo/SBA-15 catalysts are shown in Fig. 3. The bands at 1063, 965, 880 and 805 cm^{-1} are assigned to the stretching vibrations ν_{as}(P–O), ν_{as}(Mo–O_t), ν_{as}(Mo–O–Mo) and ν_{as}(Mo–O–Mo), respectively, and are characteristic of the Keggin unit [26]. Some of the bands are overlapped with the SBA-15 absorption signals, but it can be clearly seen that the bands at 965 and 805 cm^{-1} appear in the spectrum of the HPMo/SBA-15 catalyst suggesting the preservation of the Keggin structure in this calcined sample.

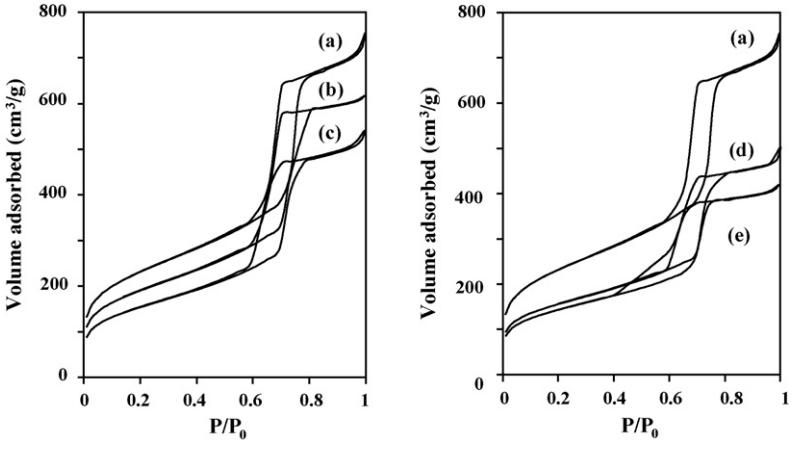

Fig. 2. Nitrogen adsorption–desorption isotherms of SBA-15 (a), NiPMo/SBA-15 (b), NiMo/SBA-15 (c), NiPW/SBA-15 (d) and NiW/SBA-15 (e).

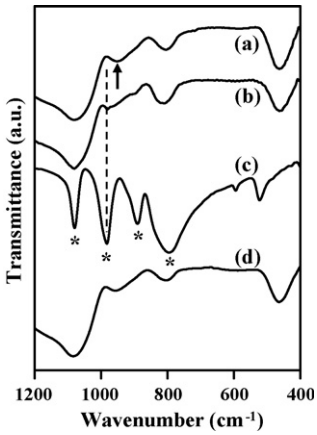

Fig. 4. IR spectra of NiPW/SBA-15 (a), HPW/SBA-15 (b), bulk $H_3PW_{12}O_{40}$ (c) and SBA-15 (d).

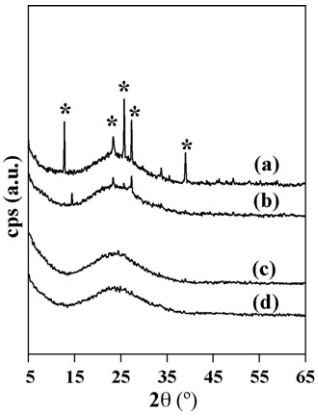

Fig. 6. XRD patterns of Mo (a), NiMo (b), HPMo (c) and NiPMo (d) catalysts supported on SBA-15. *Orthorhombic phase of MoO_3 (JCPDS card 35-609).

Promoted NiPMo/SBA-15 catalyst exhibits a spectrum similar to that of the unpromoted one, but there is a slight shift of the 965 cm^{-1} band, which now appears at ~945 cm^{-1}. Since this band is associated to the ν_{as}(Mo–O_t), the change of its position can be caused by a minor distortion of the structure due to an interaction of the Ni^{2+} cations with the terminal oxygen atoms. The same behavior (preservation of the Keggin structure in calcined HPW and NiPW catalysts and a displacement of the ν_{as}(W–O_t) band after Ni addition) can be observed for the catalysts of the HPW series (Fig. 4).

Fig. 5 shows the ^{31}P MAS NMR spectra of supported HPMo and HPW catalysts. The dried samples were kept at 100 °C for 24 h after impregnation, while the calcined ones were treated at 350 °C for 2 h. Fresh unsupported $[PW_{12}O_{40}]^{3-}$ and $[PMo_{12}O_{40}]^{3-}$ anions exhibit a characteristic chemical shift at $\delta = -14.9$ and -3.9 ppm, respectively [27]. The signals at the exactly same positions as in the precursor HPM acids can be observed in Fig. 5 for four characterized samples. Small intensity of the ^{31}P signals in the spectra in Fig. 5 is due to the low phosphorous content (0.5 wt.% of P_2O_5). The lines get broader upon calcination of the catalysts, which is caused by the loss of crystallization water from the preserved Keggin unit [18].

3.3. Characterization of the catalysts in their oxide state

Powder X-ray diffractograms for Mo-based catalysts are shown in Fig. 6. It should be mentioned that the XRD pattern of the support exhibits a broad signal caused by the amorphous silica walls of the SBA-15 material. Diffraction lines corresponding to reflections of MoO_3 in orthorhombic phase (JCPDS card 35-609) can be observed in the XRD patterns of the catalysts prepared from the conventionally used Mo precursor (AHM). This result shows that there is a poor dispersion of the oxide Mo phase in these samples, which can explain the notable loss of surface area in the NiMo/SBA-15 catalyst, probably caused by pore blockage with large MoO_3 entities. No crystalline phases were detected when the Keggin-type heteropolyacid was used as molybdenum source in the catalyst preparation. For the W series samples, the characteristic diffraction lines of the cubic phase of $H_3PW_{12}O_{40}{\cdot}6H_2O$ (JCPDS card 50-0304) were detected only in the unpromoted catalyst prepared from HPW (Fig. 7). This result not only

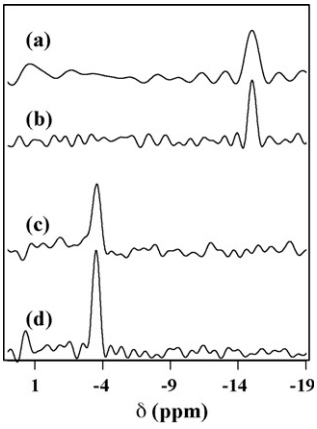

Fig. 5. ^{31}P MAS NMR spectra of HPW/SBA-15 (a and b) and HPMo/SBA-15 (c and d) catalysts. Samples (a) and (c) were calcined at 350 °C for 2 h, samples (b) and (d) were dried at 100 °C for 24 h.

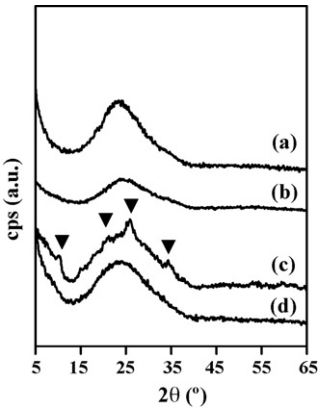

Fig. 7. XRD patterns of W (a), NiW (b), HPW (c) and NiPW (d) catalysts supported on SBA-15. (▼) Cubic phase of $H_3PW_{12}O_{40}{\cdot}6H_2O$ (JCPDS card 50-0304).

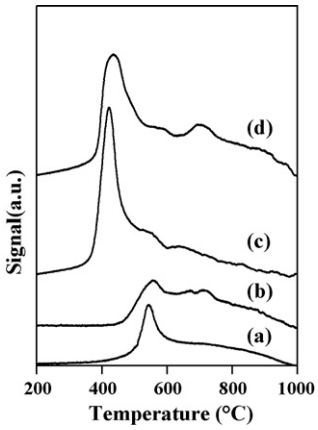

Fig. 8. TPR profiles for HPMo (a), Mo (b), NiPMo (c) and NiMo (d) catalysts supported on SBA-15.

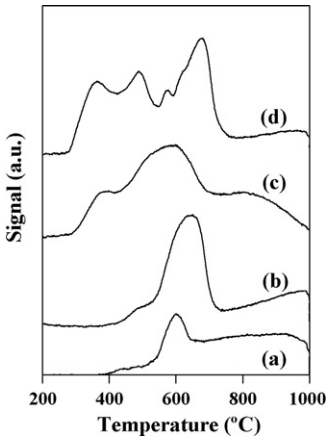

Fig. 9. TPR profiles for HPW (a), W (b), NiPW (c) and NiW (d) catalysts supported on SBA-15.

corroborates the fact that the Keggin primary structure is preserved in this catalyst after calcinations (in line with previous observations by ^{31}P MAS NMR), but also shows that the units form some crystalline aggregates which must be located outside of the SBA-15 pores. After Ni addition to the HPW/SBA-15 catalyst, the peaks no longer appear, indicating that the promoter is acting as a dispersion agent.

Reduction profiles of the molybdenum-containing catalysts are presented in Fig. 8. The reduction profile of the Mo/SBA-15 catalyst (Fig. 8, curve b) shows a complex character with three maxima at 558, 674 and 713 °C. The low-temperature hydrogen consumption (450–600 °C region) is generally associated to the first step of reduction (from Mo^{6+} to Mo^{4+}) of octahedral Mo species with different degrees of polymerization, weakly bound to the silica surface. Hydrogen consumption at 600–630 °C can be assigned to the same reduction step of the crystalline MoO_3 phase detected by XRD [28]. The peaks at 674 and 713 °C correspond to the second step of reduction of the polymeric octahedral Mo species (from Mo^{4+} to Mo^0) and to the first step of reduction of isolated tetrahedral Mo^{6+} species in strong interaction with the support. Therefore, the TPR characterization of unpromoted Mo/SBA-15 catalyst prepared using the conventional AHM precursor reveals that this sample has a mixture of octahedral Mo^{6+} species of different dispersions (from small clusters to crystalline MoO_3 phase) and tetrahedral ones. The TPR profile of HPMo/SBA-15 sample displays only one well-defined peak at 545 °C which can be assigned to the first reduction step of octahedrally coordinated Mo^{6+} in polymolybdate structure [29,30]. It can be observed that the use of $H_3PMo_{12}O_{40}$ as catalytic precursor provides a more homogeneous distribution of octahedral Mo species on the support compared to Mo/SBA-15. Yet, none of the two catalysts are expected to have a good catalytic activity due to the high temperatures required for their activation. Ni addition to Mo and HPMo/SBA-15 catalysts leads to a decrease in the reduction temperatures of molybdenum species. Thus, the TPR profile of the NiMo/SBA-15 sample exhibits two main reduction peaks at 440 and 706 °C which can be related to the first and second reduction steps of octahedral Mo species with a lower degree of polymerization than what was found for unpromoted Mo/SBA-15 sample. The shoulder at 597 °C indicates the presence of small MoO_3 crystals on the support surface as also corroborated by XRD. The TPR profile of the NiPMo/SBA-15 catalyst exhibits hydrogen consumption signals at even lower temperatures than in the previous case: at 420, 550 and 645 °C. In addition, a comparison of the four TPR profiles shown in Fig. 8 indicates that when HPMo is used as molybdenum source (instead of AHM), better-defined and sharper TPR signals are obtained pointing out a more homogeneous dispersion of Mo species in both unpromoted and Ni-promoted catalysts.

The TPR profiles of W-based catalysts are reported in Fig. 9. Unpromoted W/SBA-15 catalyst shows one well-defined reduction peak at 650 °C with a small shoulder near 490 °C, which can be assigned to the reduction of bulk WO_3 formed in the case of exceeding monolayer coverage [31]. In addition, a small hydrogen consumption above 750 °C can be observed due to the reduction of bulk-like WO_3 species, yielding $WO_{3-x\ (0<x<1)}$ suboxides with octahedrally coordinated tungsten, in accordance with the well known kinetics of the reduction process of bulk WO_3 [32]. Unpromoted HPW/SBA-15 catalyst shows TPR profile similar to that of W/SBA-15 sample. One main reduction peak is observed at about 600 °C and the presence of W species with various reducibilities is evidenced by the steady increase in the base line between 650 and 1000 °C [31]. The TPR profiles of both unpromoted W catalysts show that high temperatures (above 550 °C) are required to activate them efficiently. Ni promoter addition to the W and HPW/SBA-15 catalysts results in appearance of low-temperature reduction peaks between 300 and 500 °C. In the TPR pattern of NiW/SBA-15 catalyst a larger number of well-defined peak maxima can be observed compared to the TPR profile of NiPW/SBA-15 sample. Exact assignation of these TPR signals is complicated because of a complex character of the reduction process of W^{6+} oxide species. However, it can be clearly seen that the number and the ease of reduction of the deposited WO_3 species depends on the W source used for the catalyst preparation. It seems that in both cases (W and Mo series catalysts) a smaller number of different deposited metal species which are reduced at lower temperatures is obtained

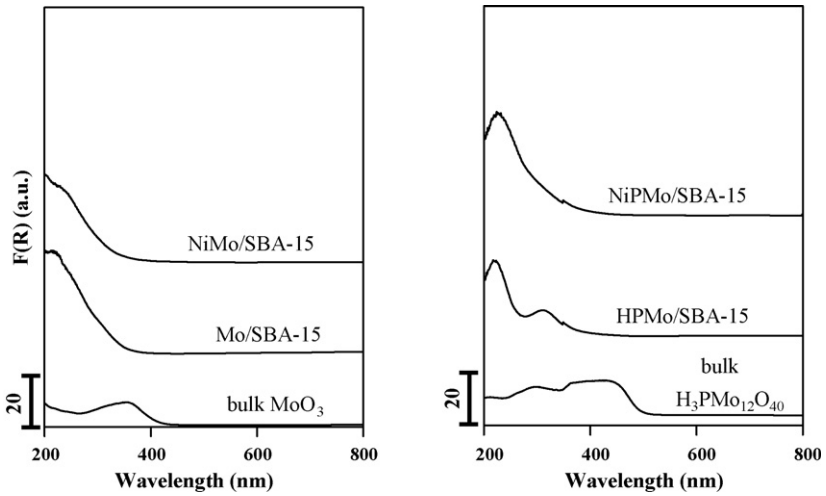

Fig. 10. UV–vis diffuse reflectance spectra of Mo catalysts and corresponding bulk compounds.

when a heteropolyacid is used as metal source instead of traditionally used ammonium salts (AHM and AMT).

Additional information about the coordination and aggregation state of Ni and Mo (W) oxide species for all catalysts was obtained by UV–vis diffuse reflectance spectroscopy. Results obtained for conventional Mo- and W-based catalysts as well as reference oxides are shown in Figs. 10 and 11. Since Mo^{6+} has a d^0 electronic configuration, only the absorption due to a ligand-to-metal charge transfer (LMCT) $O^{2-} \rightarrow Mo^{6+}$ is observed in the range of 200–400 nm. As reported elsewhere [33], the absorption bands at 260–280 and 300–320 nm are assigned to the isolated molybdate (tetrahedral) and polymolybdate (octahedral) species, respectively. In addition, both types of Mo species show the second absorption band at about 230 nm. The DR spectrum of MoO_3 sample shows the shape characteristic for this bulk-like entity [34] with the absorption edge energy (E_g) of 3.0 eV. The spectra of Mo and NiMo/SBA-15 catalysts prepared from AHM show that in both cases a mixture of Mo^{6+} ion species in tetrahedral (T_d) and octahedral (O_h) coordination is present. The absorption edge energies calculated for Mo and NiMo/SBA-15 catalysts have values of 3.3 and 3.4 eV, respectively, which show the presence of crystalline MoO_3 for both samples but also suggest that NiMo catalyst presents aggregates of smaller size.

DR spectra of W-based catalysts are presented in Fig. 11. Bulk WO_3 presents the characteristic behavior of WO_x species in an extended three-dimensional crystalline network due to LMCT transition $O^{2-} \rightarrow W^{6+}$ (O_h) and an absorption edge energy of 2.5 eV, in agreement with the reported data [35]. According to Ref. [36], the bands with maxima at 250 and 340 nm correspond to octahedral (O_h) tungsten species and the band at 275 nm to tetrahedral (T_d) tungsten entities. W and NiW/SBA-15 catalysts show a group of bands in the region of 200–350 nm which clearly suggest the presence of both species. The calculated values of E_g for W and NiW/SBA-15 catalysts are 2.8 and 3.1 eV, respectively, showing that the addition of Ni to the catalytic formulation results in a considerable reduction of WO_3 particle size.

UV–vis diffuse reflectance spectra of HPA-based catalysts are shown in Fig. 10 (Mo catalysts) and Fig. 11 (W catalysts). The spectrum of bulk $H_3PMo_{12}O_{40}$ shows the characteristic bands assigned to $O^{2-} \rightarrow Mo^{6+}$ LMCT and a band edge at about

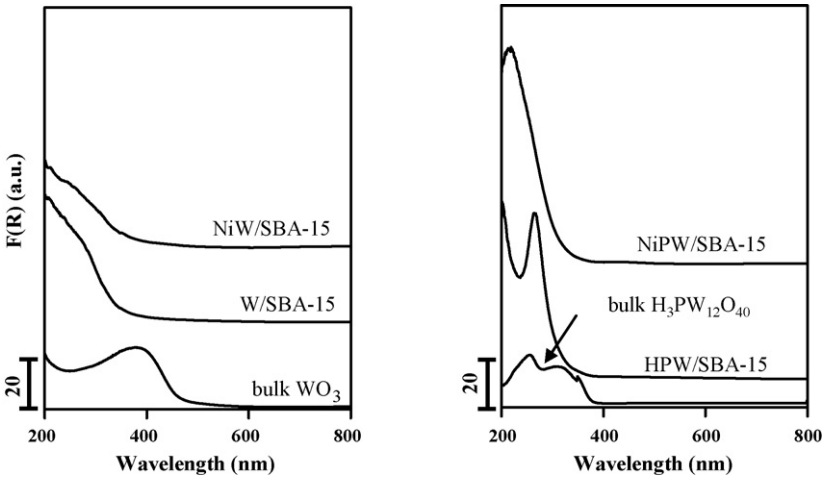

Fig. 11. UV–vis diffuse reflectance spectra of W catalysts and corresponding bulk compounds.

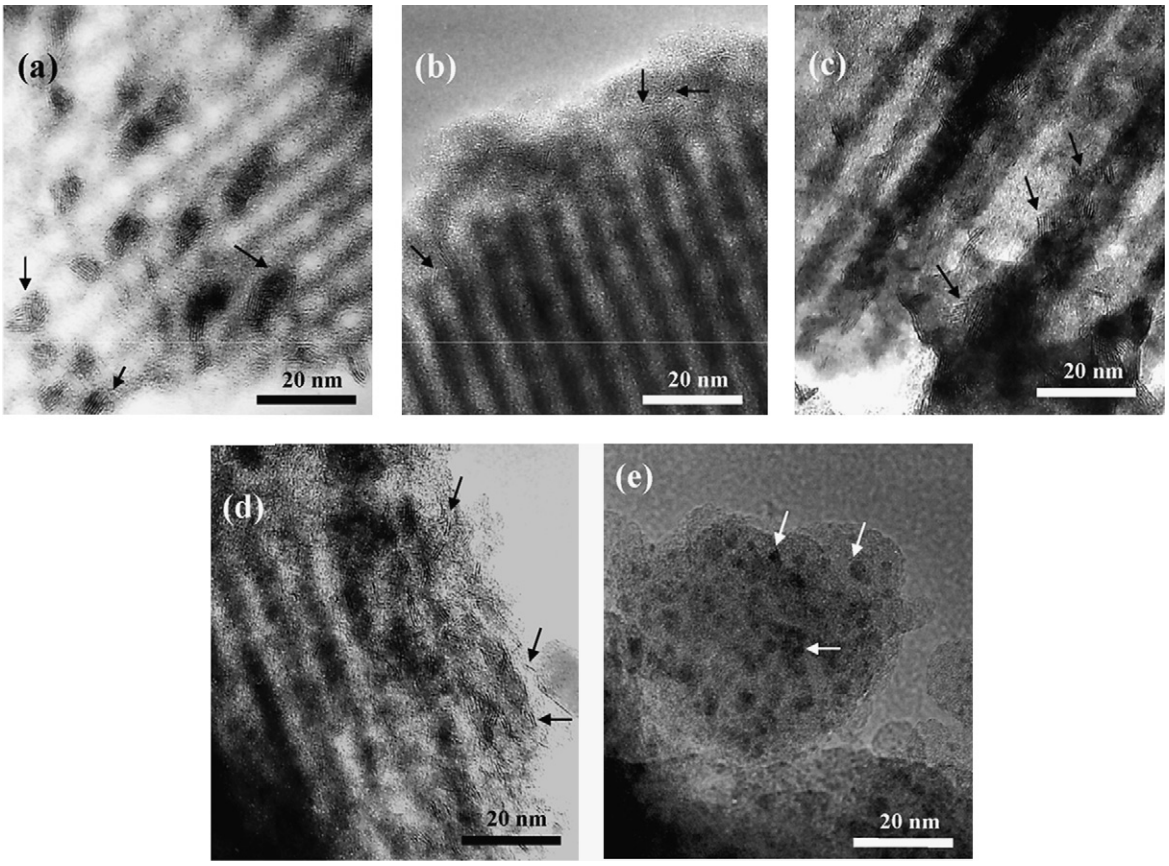

Fig. 12. HRTEM micrographs of sulfided catalysts: NiMo/SBA-15 (a), NiPMo/SBA-15 (b), NiW/SBA-15 (c) and NiPW/SBA-15 (d). The micrograph of oxided NiPW/SBA-15 catalyst (e) is also shown for comparison.

515 nm in agreement with the data reported elsewhere [37]. HPMo/SBA-15 sample shows two main signals: the first one around 220 nm and the second at 320 nm, both of which can be assigned to octahedral polymolybdate species [38]. The promoted NiPMo/SBA-15 catalyst shows only one maximum at about 240 nm. The band with maximum 320 nm (clearly observed for unpromoted catalyst) becomes less defined after Ni addition. The UV–vis electronic spectrum exhibited by bulk $H_3PW_{12}O_{40}$ consists of a broad group of signals of $O^{2-} \rightarrow W^{6+}$ charge transfer with two maxima (at about 250 and 330 nm) and an absorption edge at about 400 nm, which is in agreement with the literature [37,39,40]. SBA-15-supported HPW shows one well-defined maximum at 264 nm attributable to an $O^{2-} \rightarrow W^{6+}$ intraframework ($W_{12}O_{36}$) charge transfer in the highly dispersed Keggin units [39]. In the DR spectrum of NiPW/SBA-15 catalyst this signal is blue-shifted indicating an increase in the dispersion of W species. A comparison of the absorption edge energies of the NiMo and NiW/SBA-15 catalysts prepared from AHM and AMT with those of NiPMo and NiPW/SBA-15 samples (3.6 and 3.8 eV, respectively) points out a better dispersion of metal species in the catalysts prepared using HPA precursors. Also when HPAs are used, sharper and better-defined absorption bands are seen in the spectra of unpromoted and Ni-promoted catalysts probably because of a more homogeneous distribution of Mo and W species. Finally, DRS characterization of Ni-promoted catalysts showed in all the cases the presence of octahedral Ni species in the form of NiO (band at 720 nm, not shown).

3.4. HRTEM of sulfided catalysts

In order to get information about the dispersion of the activated catalysts, HRTEM studies were performed. The typical fringes due to MoS_2 or WS_2 crystallites with 6.2 Å interplanar distances were observed on micrographs of all sulfided catalysts (Fig. 12), showing that the Keggin units were transformed during the sulfidation stage to the sulfided Mo (W) phase with regular structure. This transformation can be corroborated by comparing the micrographs of the sulfided catalysts with the corresponding ones of the oxided catalysts. For example, Fig. 12(e) shows the micrograph of the oxided NiPW/SBA-15 sample in which the Keggin units can be seen as small round particles distributed over the support. The distributions in stacking degree and slab length for the different catalysts are presented in Fig. 13. Both Mo and W catalysts show a better dispersion (smaller average stacking degree and slab length) when HPAs were used as precursors (Figs. 12 and 13). NiMo/SBA-15 sample shows an average of four layers and an average slab length of 45 Å, while the sulfided phase of NiPMo/SBA-15 catalyst consists mostly of two- to three-layered crystals with 25–35 Å length. Similar changes in the sulfided phase morphology can also be clearly observed for the

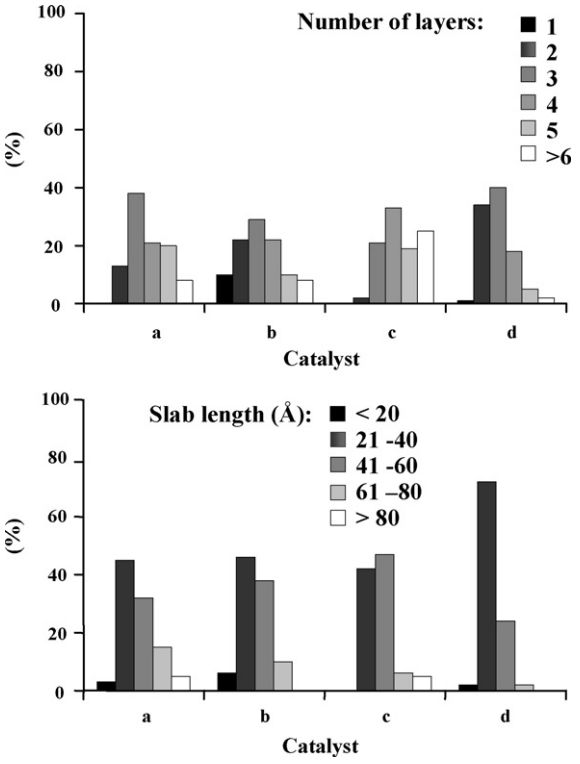

Fig. 13. Layer stacking and length distribution of MS_2 crystallites in sulfided NiMo (a), NiPMo (b), NiW (c) and NiPW (d) catalysts supported on SBA-15.

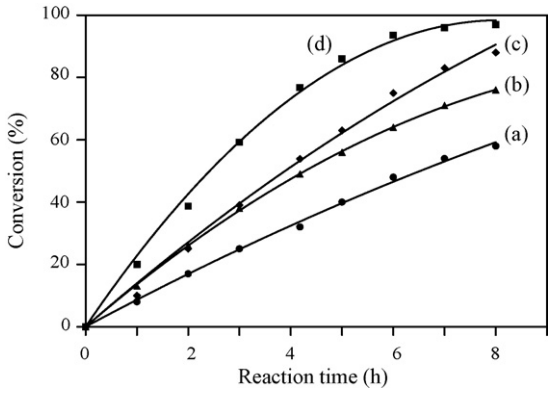

Fig. 14. 4,6-DMDBT conversions obtained over NiMo (a), NiPMo (b), NiW (c) and NiPW (d) catalysts supported on SBA-15.

W series catalysts. On the micrograph of the sulfided NiW/SBA-15 catalyst, larger (50–60 Å length) and more stacked (two to eight layers) crystals are seen than in the case of the sulfided NiPW/SBA-15 sample. These results show that the use of HPA precursor results in both cases (Mo and W series catalysts) in a considerable increase in the dispersion of MS_2 active phase. Moreover, it can be clearly seen from Figs. 12 and 13 that NiMo/SBA-15 and NiW/SBA-15 samples present a very inhomogeneous dispersion of the MS_2 phase compared to their respective NiPM analogues.

3.5. Catalytic activity

It is well known that in order to reach a significant reduction in sulfur content in hydrotreated gas oil fractions (from 500 to less than 50 ppm) it is necessary to remove the most refractory compounds. So in the present study, 4,6-dimethyldibenzothiophene was selected as a relevant probe molecule [1,41] to determine the catalytic activity of the sulfided catalysts in deep HDS. The conversions of 4,6-DMDBT obtained over Ni-promoted Mo and W catalysts are shown in Fig. 14. Catalytic activities of all NiPM/SBA-15 catalysts resulted to be significantly higher than those of their analogues prepared with conventional precursors. The lowest 4,6-DMDBT conversion was observed for NiMo/SBA-15 catalyst (58% at 8 h), while the conversion obtained with NiPMo/SBA-15 catalyst with the same Ni and Mo loadings was about 20% higher (72% at 8 h). A similar behavior was also observed for the W series catalysts (97% conversion at 8 h for NiPW/SBA-15 catalyst and 88% for the corresponding NiW one). Pseudo-first-order rate constants (k_1 expressed in l/(s $g_{catalyst}$)) determined for the different catalysts (Table 2) vary between 8.0×10^{-6} and 3.2×10^{-5} l/(s $g_{catalyst}$) and also confirm the following order of activity: NiPW/SBA-15 > NiW/SBA-15 > NiPMo/SBA-15 > NiMo/SBA-15. It is worth mentioning that all the constants determined in the present study are substantially higher than that reported previously for a reference NiMo/γ-Al_2O_3 catalyst tested in 4,6-DMDBT HDS under similar reaction conditions (5.18×10^{-6} l/(s $g_{catalyst}$)) [38]. The rate constants k_1 were also calculated in terms of metal content (l/(s mol MO_3)). It can be seen in Table 2 that both tungsten-based catalysts show a better performance than their respective Mo-based analogues loaded with the same molar amount of each oxide. This result helps us point out that even though CoMo and NiMo sulfides have attracted most of the attention for HDT applications, the limitations for using W-based catalysts (i.e. high sulfidation temperatures caused by a strong interaction with the alumina support [42]) can be overcome by using other supports (like carbon [42], titania [43] or in this case, SBA-15) and the cost factors which also limit the application of W might be traduced into a gain in sulfur removal.

Generally, there are two reaction pathways for the HDS reaction of methyl-substituted DBT derivatives. The first one is the direct elimination of the sulfur atom from the molecule (DDS route) yielding the corresponding substituted biphenyl products, and the second one is the prehydrogenation of one aromatic ring followed by elimination of the sulfur atom (HYD

Table 2
Pseudo-first-order rate constants and HYD/DDS pathway ratios obtained for 4,6-DMDBT HDS over promoted catalysts[a]

Catalyst	k_1 (l/(s $g_{catalyst}$))	k_1 (l/(s mol MO_3))	HYD/DDS ratio[b]
NiMo/SBA-15	8.0×10^{-6}	9.6×10^{-3}	6.1
NiPMo/SBA-15	1.3×10^{-5}	1.6×10^{-2}	7.8
NiW/SBA-15	2.6×10^{-5}	3.0×10^{-2}	6.7
NiPW/SBA-15	3.2×10^{-5}	3.7×10^{-2}	10.3

[a] Batch reactor, 40 ml of 4,6-DMDBT solution in n-hexadecane (0.0124 mol/l), 0.15 g of catalyst, 300 °C, 7.3 MPa.
[b] Determined at 50% of total 4,6-DMDBT conversion. DDS, direct desulfurization pathway; HYD, hydrogenation pathway. HYD/DDS pathway ratio was determined as the ratio of HYD route main product (methylcyclohexyltoluene) to DDS route product (dimethylbiphenyl).

route), yielding first substituted tetrahydro- and hexahydrodibenzothiophenes and then the corresponding cyclohexylbenzene-type compounds [44]. In order to elucidate the effect of using HPA-type precursors on the reaction pathways of 4,6-DMDBT, the reaction product distributions at the same total conversion (50%) were compared for the different catalysts (Table 2). The HYD/DDS ratios determined as the ratios of the main desulfurized products obtained in each route (methylcyclohexyltoluene/dimethylbiphenyl, respectively) show that for all the catalysts studied the preferential pathway is HYD. As expected [45], W-based catalysts show a higher hydrogenation capability than their respective Mo-based analogues. However, the catalysts prepared using HPA precursors show a higher preference for the HYD route compared to the conventional NiM catalysts (M = Mo, W). The maximum HYD/DDS (10.3) is reached by the most active catalyst, NiPW/SBA-15. These results suggest that the use of HPAs as catalyst precursors leads to an improvement in the hydrogenation ability of the catalyst, enhancing HYD route which results in an overall increase in the rate of 4,6-DMDBT HDS. This conclusion can be partially explained in terms of catalyst morphology. For the sulfided catalysts where HPAs were used as precursors, a homogeneous distribution of MS_2 crystals can be observed (Figs. 12 and 13). These consist mostly of two or three layers and about 25–35 Å in length, where NiPW catalyst presents the shortest slabs (less than 30 Å). Crystals with similar characteristics have been observed to present a favorable slab length/layer stacking ratio for hydrodesulfurization of 4,6-DMDBT due to an enhancement of HYD route [38].

4. Discussion

It clearly appears that the use of Keggin-type HPAs as starting materials in the preparation of the catalysts has a beneficial effect on their activity. In a first attempt to explain this phenomenon, we may address the presence of phosphorus in the precursor of the active phase used. Nowadays, it is well known that phosphorus addition in HDS catalysts improves their catalytic activity [8]. Atanasova et al. [46] found that the effect of phosphorus addition depends on the method used for its incorporation to the catalyst, being the positive effects of P better expressed when incorporated to the support in the first impregnation step rather than simultaneously with the other oxide precursor salts. Even though most of the reports about P addition to HDS catalysts deal with alumina-supported entities, recently it has also been shown that the addition of small amounts of phosphorus (about 1 wt.% P_2O_5) in the NiMo/MCM-41 catalysts leads to an increase in 4,6-DMDBT conversion from 73 to 84% at 8 h reaction time [47]. It was found that phosphorus addition produces some changes in the morphology of the active MoS_2 and promotes the hydrogenation pathway of HDS. In the present work, not only the phosphorus content in the catalysts is twice smaller than in the reference cited above [47] (barely 0.5 wt.% of P_2O_5) but the incorporation of this additive was performed in the same impregnation step as Mo and W. However, a significant change in the catalytic activity can be clearly observed when Keggin-type heteropolyacids are used instead of traditionally employed ammonium salts (AMT and AHM) (Table 2; Fig. 14). On the other hand, the results obtained by Griboval et al. [17], who compared catalytic activities of the two series of CoMo catalysts, one prepared using silicium and other phosphorus heteropolycompounds (HPC), show that the catalysts of both series have similar activity in HDS of thiophene. It seems that the original structure of the starting material used, in this case of the Keggin-type HPA units, is more important for the behavior of the HDS catalysts, than the nature of the atom it has in the center. Taking these arguments into account, we should conclude that the good catalytic behavior of our catalysts prepared using HPAs as precursors should not be attributed to the presence of phosphorus itself, but to the capability of this atom to keep small units of Mo (W) oxides together in close proximity and form aggregates of a defined size and homogeneous distribution (i.e. the Keggin unit).

Results from the TPR, DRS and XRD characterization of the NiM and NiPM/SBA-15 catalysts in their oxide state point out that a better dispersion and a more uniform distribution of metal species are obtained when the HPAs are used as precursors. Even the N_2 physisorption data show that the HPA-based catalysts have better textural properties and less pore blockage produced by large oxide entities inside and on the entrances of the mesopores compared to the traditional catalysts. IR and ^{31}P MAS NMR spectra of oxide catalysts indicate that the characteristic Keggin structure of the HPMo and HPW precursors was preserved during the impregnation of SBA-15 and subsequent drying and calcination steps. This behavior is different from the reported previously for the Keggin-type units supported on Al_2O_3, which were decomposed in similar conditions due to very strong interaction with alumina [14]. When SBA-15 is used as a support, the interaction of HPA moieties with the support surface is much weaker. This, in addition to good thermal stability of the used HPAs, seems to be the reason for the preservation of the Keggin structure in SBA-15-supported precursors. The results here above, all together, allow us to conclude that a more uniform distribution of relatively small starting units should be obtained on SBA-15 surface when heteropolyacids are used in the catalyst preparation instead of ammonium heptamolybdate or ammonium metatungstate. According to the results of characterization of the sulfided catalysts by HRTEM, a good dispersion of metal species in the oxide state of the catalyst leads to better dispersed active phases, which is a necessary condition for the creation of a larger amount of accessible active sites improving catalytic activity.

Finally, it was observed that the nickel promoter also plays an important role in the enhancement of catalytic activity of the NiPM/SBA-15 catalysts. Previously, it has already been reported that either unpromoted HPMo (HPW) catalysts or promoted with small amounts of Co(Ni) ones have low HDS activity [19,22]. Our present results show that when Ni is added to the catalytic formulations, important changes occur. First, nickel significantly improves dispersion of the deposited HPA species. This can be clearly observed in the case of HPW, where the few HPW crystals detected by XRD disappear after adding the promoter. DRS results also show that the promoted oxide precursors have smaller particle size compared to the

unpromoted analogues in all cases. The presence of Ni also results in the appearance of oxide Mo (W) species susceptible to be reduced at lower temperatures (TPR), which should also make the active phase easier to sulfide. Even though there is the evidence for thinking that Ni atoms are directly interacting with the terminal oxygen atoms of the Keggin entity (FT-IR), further characterization is needed to prove this statement. We also think that this kind of interaction between Ni and Mo (W) in the oxide precursor is the key for obtaining an appropriate sulfided phase in which the number and type of NiMo(W)S active sites is optimized and allows the 4,6-DMDBT molecule to be hydrogenated better in order to yield less hindered intermediates in which sulfur elimination becomes easier.

5. Conclusions

In the present work, two series of Mo (W) catalysts promoted by Ni and supported on pure siliceous SBA-15 were prepared: the first one using Keggin-type heteropolyacids ($H_3PMo_{12}O_{40}$ or $H_3PW_{12}O_{40}$) as active phase precursors, and the second from the traditional precursors (ammonium heptamolybdate, ammonium metatungstate). Prepared catalysts were characterized by N_2 physisorption, small- and wide-angle XRD, UV–vis DRS, FT-IR, TPR, ^{31}P MAS NMR, HRTEM and evaluated in hydrodesulfurization of 4,6-DMDBT. Obtained results allow us to conclude the following.

Both NiPMo and NiPW/SBA-15 catalysts prepared from corresponding heteropolyacids showed better performance in deep HDS of 4,6-DMDBT than their counterparts prepared from the traditionally used Mo (W) ammonium salts. The reason for the high catalytic activity of the NiPM/SBA-15 formulations seems to be related to the specific structure of the Keggin-type precursor rather than to the presence of a phosphorus atom in its center.

The weak interaction of HPA with pure siliceous SBA-15 surface is beneficial for the integrity of the Keggin-type anions preventing their decomposition during all the steps of the catalyst preparation.

The use of heteropolyacids as active metal sources leads to better dispersion and more homogeneous distribution of oxided and sulfided Mo and W species compared to that obtained from ammonium heptamolybdate and ammonium metatungstate. Similar trends are also observed for the sulfided catalysts, showing that the well-dispersed sulfided HDS catalysts can be obtained only from the well-dispersed corresponding oxide counterparts.

Acknowledgements

Financial support by DGAPA-UNAM (grant IN-104106) is gratefully acknowledged. The authors thank M. Aguilar, I. Puente and C. Salcedo for technical assistance.

References

[1] K.G. Knudsen, B.H. Cooper, H. Topsøe, Appl. Catal. A 189 (1999) 205–215.
[2] C. Song, Catal. Today 86 (2003) 211–263.
[3] G. Murali Dhar, B.N. Srinivas, M.S. Rana, M. Kumar, S.K. Maity, Catal. Today 86 (2003) 45–60.
[4] A. Niquille-Röthlisberger, R. Prins, J. Catal. 242 (2006) 207–216.
[5] S. Ramanathan, C.C. Yu, S.T. Oyama, J. Catal. 173 (1998) 10–16.
[6] P. Clark, W. Li, S.T. Oyama, J. Catal. 200 (2001) 140–147.
[7] M. Breysse, P. Afanasiev, C. Geantet, M. Vrinat, Catal. Today 86 (2003) 5–16.
[8] H. Topsøe, S. Clausen, F.E. Massoth, Hydrotreating Catalysis Science and Technology, Springer, Berlin, 1996.
[9] C. Kwak, M.Y. Kim, K. Choi, S.H. Moon, Appl. Catal. A 185 (1999) 19–27.
[10] N. Mizuno, M. Misono, Chem. Rev. 98 (1998) 199–218.
[11] I.V. Kozhevnikov, J. Mol. Catal. A 262 (2007) 86–92.
[12] S. Damyanova, J.L.G. Fierro, Appl. Catal. A 144 (1996) 59–77.
[13] A. Grivobal, P. Blanchard, E. Payen, M. Fournier, J.L. Dubois, Chem. Lett. 12 (1997) 1259–1260.
[14] A. Griboval, P. Blanchard, E. Payen, M. Fournier, J.L. Dubois, Catal. Today 45 (1998) 277–283.
[15] A. Griboval, P. Blanchard, L. Gengembre, E. Payen, M. Fournier, J.L. Dubois, J.R. Bernard, J. Catal. 188 (1999) 102–110.
[16] R. Shafi, M. Rafiq, H. Siddiqui, G.J. Hutchings, E.G. Derouane, I.V. Kozhevnikov, Appl. Catal. A 204 (2000) 251–256.
[17] A. Griboval, P. Blanchard, E. Payen, M. Fournier, J.L. Dubois, J.R. Bernard, Appl. Catal. A 217 (2001) 173–183.
[18] B. Pawelec, S. Damyanova, R. Mariscal, J.L.G. Fierro, I. Sobrados, J. Sanz, L. Petrov, J. Catal. 223 (2004) 86–97.
[19] P. Blanchard, C. Lamonier, A. Griboval, E. Payen, Appl. Catal. A 322 (2007) 33–45.
[20] D. Zhao, Q. Huo, J. Feng, B.F. Chmelka, G.D. Stucky, J. Am. Chem. Soc. 120 (1998) 6024–6036.
[21] D. Zhao, J. Feng, Q. Huo, N. Melosh, G.H. Fredrickson, B.F. Chmelka, G.D. Stucky, Science 279 (1998) 548–552.
[22] L. Lizama, J.C. Amezcua, R. Reséndiz, S. Guzmán, G.A. Fuentes, T. Klimova, Stud. Surf. Sci. Catal. 165 (2007) 799–802.
[23] I.V. Kozhevnikov, Chem. Rev. 98 (1998) 171–198.
[24] V.B. Fenelonov, V.N. Romannikov, A.Y. Derevyankin, Micropor. Mesopor. Mater. 28 (1999) 57–72.
[25] L. Marosi, E. Escalona Platero, J. Cifre, C. Otero Areán, J. Mater. Chem. 10 (2000) 1949–1955.
[26] A.J. Bridgeman, G. Cavigliasso, J. Phys. Chem. A 107 (2003) 6613–6621.
[27] R. Massart, R. Contant, J.M. Fruchart, J.P. Ciabrini, M. Fournier, Inorg. Chem. 16 (1977) 2916–2921.
[28] T. Klimova, L. Lizama, J.C. Amezcua, P. Roquero, E. Terrés, J. Navarrete, J.M. Domínguez, Catal. Today 98 (2004) 141–150.
[29] S. Damyanova, M.L. Cubeiro, J.L.G. Fierro, J. Mol. Catal. A 142 (1999) 85–100.
[30] N.G. Kostova, A.A. Spojakina, K. Jiratova, O. Solcova, L.D. Dimitrov, L.A. Petrov, Catal. Today 65 (2001) 217–223.
[31] C.H. Kim, W.L. Yoon, I.C. Lee, S.I. Woo, Appl. Catal. A 144 (1996) 159–175.
[32] V. Logie, G. Maire, D. Michel, J.-L. Vignes, J. Catal. 188 (1999) 90–101.
[33] Z. Liu, Y. Chen, J. Catal. 177 (1998) 314–324.
[34] R.S. Weber, J. Catal. 151 (1995) 470–474.
[35] D.G. Barton, M. Shtein, R.D. Wilson, S.L. Soled, E. Iglesia, J. Phys. Chem. B 103 (1999) 630–640.
[36] B. Scheffer, J.J. Heijeinga, J.A. Moulijn, J. Phys. Chem. 91 (1987) 4752–4759.
[37] K.P. Barteau, J.E. Lyons, I.K. Song, M.A. Barteau, Top. Catal. 41 (2006) 55–62.
[38] O.Y. Gutiérrez, G.A. Fuentes, C. Salcedo, T. Klimova, Catal. Today 116 (2006) 485–497.
[39] Y.R. Guo, Q.J. Pan, Y.D. Wei, Z.H. Li, X. Li, J. Mol. Struct. (Theochem) 676 (2004) 55–64.
[40] M.H. Youn, H. Kim, J.C. Jung, I.K. Song, K.P. Barteau, M.A. Barteau, J. Mol. Catal. A 241 (2005) 227–232.
[41] B.C. Gates, H. Topsøe, Polyhedron 16 (1997) 3213–3217.
[42] E.J.M. Hensen, Y. van der Meer, J.A.R. van Veen, J.W. Niemantsverdriet, Appl. Catal. A 322 (2007) 16–32.

[43] M.J. Vissenberg, Y. van der Meer, E.J.M. Hensen, V.H.J. de Beer, A.M. van der Kraan, R.A. van Santen, J.A.R. van Veen, J. Catal. 198 (2001) 151–163.
[44] F. Bataille, J.L. Lemberton, P. Michaud, G. Pérot, M. Vrinat, M. Lemaire, E. Schulz, M. Breysse, S. Kasztelan, J. Catal. 191 (2000) 409–422.
[45] S.K. Bej, S.K. Maity, U.T. Turaga, Energy Fuels 18 (2004) 1227–1237.
[46] P. Atanasova, T. Tabakova, Ch. Vladov, T. Halachev, A. Lopez Agudo, Appl. Catal. A 189 (1997) 105–119.
[47] J.M. Herrera, J. Reyes, P. Roquero, T. Klimova, Micropor. Mesopor. Mater. 83 (2005) 283–291.